LETTER Communicated by John Rinzel

Spike Frequency Adaptation Affects the Synchronization Properties of Networks of Cortical Oscillators

Sharon M. Crook
Center for Computational Biology, Montana State University, Bozeman, MT 59717, U.S.A.

G. Bard Ermentrout
Department of Mathematics, University of Pittsburgh, Pittsburgh, PA 15260, U.S.A.

James M. Bower
Division of Biology, California Institute of Technology, Pasadena, CA 91125, U.S.A.

Oscillations in many regions of the cortex have common temporal characteristics with dominant frequencies centered around the 40 Hz (gamma) frequency range and the 5–10 Hz (theta) frequency range. Experimental results also reveal spatially synchronous oscillations, which are stimulus dependent (Gray & Singer, 1987; Gray, König, Engel, & Singer, 1989; Engel, König, Kreiter, Schillen, & Singer, 1992). This rhythmic activity suggests that the coherence of neural populations is a crucial feature of cortical dynamics (Gray, 1994). Using both simulations and a theoretical coupled oscillator approach, we demonstrate that the spike frequency adaptation seen in many pyramidal cells plays a subtle but important role in the dynamics of cortical networks. Without adaptation, excitatory connections among model pyramidal cells are desynchronizing. However, the slow processes associated with adaptation encourage stable synchronous behavior.

1 Introduction

There is great interest in the mechanisms underlying the oscillatory properties of networks of cortical cells (Gray, 1994). In particular, there are many questions about which properties encourage synchrony, traveling waves of oscillations, or other phase shifts in phase-locked activity that may be computationally significant (Gray & Singer, 1989; Bressler, 1984; Freeman, 1978; Bower, 1995). In this article, we briefly describe a biophysically based compartmental model of an adapting cortical pyramidal cell. Then we use this model to derive a simpler coupled oscillator model that provides insight into the synchronizing properties of networks of cortical oscillators. We verify the predictions of the coupled oscillator model using simulations of networks of the biophysically based model.

In general, biophysical models of excitable membrane usually represent the dynamics of a cell in the general Hodgkin and Huxley (1952) current balance format,

$$C_M \frac{dV(t)}{dt} = -I_{Ion}(V, \vec{w}) + I_{Stim}(t), \tag{1.1}$$

where $V(t)$ denotes the deviation of the membrane potential from some reference potential at time t, I_{Ion} is the sum of voltage and time-dependent currents through the various ionic channel types, and $\vec{w}$ is the vector of auxiliary membrane variables such as intracellular calcium and the gating variables. The stimulus $I_{Stim}(t)$ represents the electrode current applied to the soma divided by the total cell membrane area. Membrane potential $V(t)$ is in units of mV, membrane capacitance C_M is in units of μF/cm^2, currents are densities with units of μA/cm^2, the time unit is ms, and the gating variables appearing in $\vec{w}$ describe the fraction of channels of a given type that are in various conducting states at time t.

When a more complex spatially distributed model is necessary, a cell model is usually constructed of smaller compartments, which are assumed to be isopotential with uniform physical properties (Segev, Fleshman, & Burke, 1992). In this case, there is a system of current balance equations similar to equation 1.1 that reflect the membrane properties of each particular somatic or dendritic compartment, including any ionic currents, synaptic inputs, and applied currents. Additional terms are included to represent the longitudinal currents flowing between neighboring compartments.

In contrast, coupled oscillator models provide a simplified approach that can be useful for representing networks of cells by reducing the number of required equations and providing a context for a more analytical approach. Coupled oscillator models use a single phase variable to approximate the voltage oscillation of each neuron or neural assembly during repetitive firing. The behavior of a pair of coupled oscillators depends critically on the single interaction function chosen to represent the coupling between them.

The behavior of our biophysically based compartmental model of an adapting pyramidal cell very closely matches experimental current clamp data from a brain slice preparation of rat piriform cortex (Crook, Ermentrout, Vanier, & Bower, 1997). We use this compartmental model to derive interaction functions that approximate the coupling for pairs of pyramidal cells. Since the interaction functions are derived from the biophysically based model rather than being chosen arbitrarily, they provide an accurate approximation, provide insight into the behavior of networks of coupled pyramidal cells, and illuminate conditions that encourage synchronous oscillations. We are able to verify the behavioral predictions of the coupled oscillator approach with simulations performed for a network comprised of the biophysically based compartmental pyramidal cell model.

2 Compartmental Model

Action potentials produced by pyramidal cells often occur at a higher frequency during the initial stages of the current injection, with a decreased firing rate at later stages of a sustained injection (Connors, Gutnick, & Prince, 1982; Madison & Nicoll, 1984). Experimental evidence shows that this spike frequency adaptation can be partially suppressed by application of acetylcholine or norepinephrine, which block various potassium currents (Sherman & Koch, 1986; Steriade and Llinas, 1988). Thus, the degree of adaptation is partially determined by the ionic conductance density of the currents responsible for adaptation. The hyperpolarization of the membrane potential due to potassium efflux regulates the firing rate by establishing a relative refractory period for the neuron. Thus, the degree of adaptation also depends on the relative timing of the kinetics of the adaptation currents and on the rate of decay of intracellular calcium, as described by Crook and Ermentrout (1997).

We initially developed an adapting pyramidal cell model with one somatic compartment and four dendritic compartments using a current balance equation for each of the five compartments. Additional equations were used to represent the dynamics of the gating variables for the various ionic currents in the soma. The parameters representing the maximal conductances of the ion channels as well as the kinetic parameters were systematically adjusted using an automated parameter search method (Vanier & Bower, 1996). The resulting model accurately reproduces the experimental spiking behavior from a brain slice preparation of rat piriform cortex for a wide range of injected currents (Crook et al., 1997). Then we reduced the five-compartment model to a two-compartment model in the manner of Pinsky and Rinzel (1994). In the reduced model, a single compartment represents the entire dendritic structure; however, the model demonstrates the same qualitative behavior with the same level of accuracy as the full model (Crook, 1996). The currents in the model include a fast-activating voltage-dependent sodium current (I_{Na}) and a delayed rectifier potassium current (I_{K-DR}) mediating the generation of simulated action potentials. The model also includes two different currents that contribute to the spike frequency adaptation. One is a noninactivating voltage-dependent potassium current (I_{K-M}), and the other is a calcium-dependent potassium current (I_{K-AHP}). There is also a high-threshold voltage-activated calcium current (I_{Ca}) similar to those in other pyramidal cell models (Barkai & Hasselmo, 1994; Traub, Wong, Miles, & Michelson, 1991; Pinsky & Rinzel, 1994). The standard voltage-independent leak currents (I_{L-S} and I_{L-D}) are included where the current in the soma partially reflects impalement damage. Equations and parameters for the reduced model are provided in the appendix.

Experimental evidence shows that after spike frequency adaptation has occurred, pyramidal cells can exhibit oscillations at very low frequencies near the critical applied current required for the onset of repetitive firing

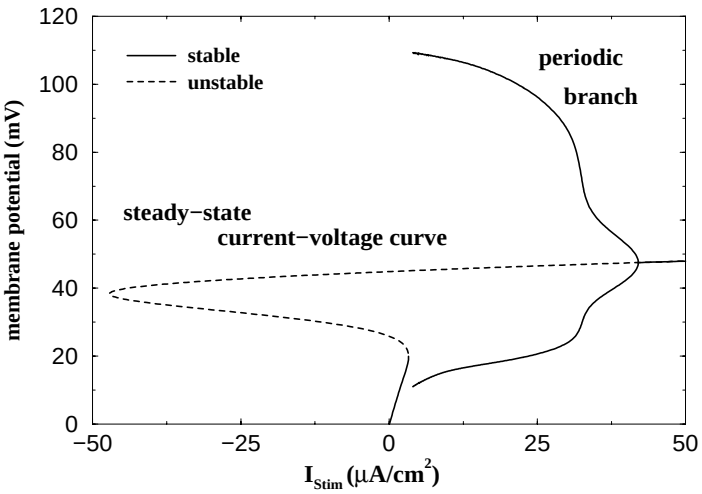

Figure 1: Bifurcation diagram for the adapting pyramidal cell model showing current injection (I_{Stim} μA/cm^2) versus membrane voltage deviation from rest (mV). For low current injection values, the cell demonstrates steady-state behavior, as suggested by the stable portion of the steady-state current voltage curve shown solid. At $I_{Stim} \approx 3.28$ μA/cm^2 a saddle node bifurcation occurs so that at higher current injection values, the cell demonstrates repetitive firing. The periodic branch shows the maximum and minimum voltage of the oscillation produced by a given value of I_{Stim}. The diagram depicts the behavior after adaptation has occurred.

(Lanthorn, Storm, & Andersen, 1984; McCormick, Connors, Lighthall, & Prince, 1985; Haberly, 1985; Barkai & Hasselmo, 1994). This behavior is characteristic of membrane models where the transition to repetitive firing occurs due to a saddle node bifurcation. Such models are known as type I membrane models (Rinzel & Ermentrout, 1992). Our biophysical pyramidal cell model demonstrates the characteristic low frequencies typical of type I membranes, and we verify that repetitive firing occurs due to the presence of a saddle node bifurcation, as shown in Figure 1.

3 Coupled Oscillator Model

Network simulations using coupled biophysically based cell models provide a valuable tool for exploring the effects of different parameters. However, the dynamics underlying the network behavior are often obscured by the complicated nature of the model cells. Consider any cortical oscillator

where the dynamics of the cell can be represented by equation 1.1, with an additional term representing a synaptic current. We can assume that the stimulus I_{Stim} is constant and spatially homogeneous so that the neuron is capable of spontaneously oscillating in the absence of synaptic current (Rinzel & Ermentrout, 1992). Alternatively, one can hypothesize that the cell acts as an oscillator due to the local network interactions with inhibitory neurons, as described in various models of cortical networks (Eeckman & Freeman, 1990; Whittington, Traub, & Jefferys, 1995; Wilson & Bower, 1991, 1992). In either case, $V(t)$ denotes the oscillation of a single uncoupled oscillator so that $V(t)$ can be approximated by $V(\theta(t))$ where $\theta(t)$ represents the periodic phase of the oscillator. The phase variable $\theta(t)$ lies in the interval $[0, T]$ where T is the period of the oscillation. If the intrinsic frequency of the oscillator is ω, then the phase satisfies

$$\frac{d\theta(t)}{dt} = \omega. \tag{3.1}$$

This single-variable phase model approximates the repetitive behavior of the voltage oscillation, but no amplitude information is retained.

3.1 Interaction Function. A synaptic current with no delay or spatial dependence has the form

$$I_{Syn}(t) = \bar{g}_{Syn} S[\hat{V}(t)](V(t) - V_{Syn}), \tag{3.2}$$

where $\bar{g}_{Syn}$ denotes the maximal conductance for the synapse, V_{Syn} is the synaptic reversal potential, and $S[\cdot]$ is some functional of the presynaptic voltage $\hat{V}(t)$, which provides the synaptic time course and is equivalent to an alpha function or dual exponential. Now consider two oscillators identical to those of equation 1.1 that are coupled symmetrically with no delay or spatial dependence:

$$C\frac{dV_1(t)}{dt} = -I_{Ion}(V_1, \vec{w}_1) + I_{Stim} - \bar{g}_{Syn} S[V_2(t)](V_1(t) - V_{Syn}) \tag{3.3}$$

$$C\frac{dV_2(t)}{dt} = -I_{Ion}(V_2, \vec{w}_2) + I_{Stim} - \bar{g}_{Syn} S[V_1(t)](V_2(t) - V_{Syn}). \tag{3.4}$$

If $\bar{g}_{Syn}$ is small, then it is possible to average the equations, leading to a phase model for the interactions between the neurons (Ermentrout & Kopell, 1984; Kuramoto, 1984). This phase reduction approach has been used by numerous authors in order to understand the dynamics of interacting neural oscillators where the coupling is weak (Ermentrout & Kopell, 1991; Cohen et al., 1992). The phases of the oscillators in this coupled system satisfy

$$\frac{d\theta_1(t)}{dt} = \omega + \bar{g} H(\theta_2(t) - \theta_1(t)) \tag{3.5}$$

$$\frac{d\theta_2(t)}{dt} = \omega + \bar{g}H(\theta_1(t) - \theta_2(t)), \tag{3.6}$$

where $\bar{g}$ denotes the coupling strength, and the interaction function $H(\cdot)$ is periodic and is determined by the form of the synaptic coupling and the nature of the uncoupled oscillation (Ermentrout & Kopell, 1990). Note that the interaction function depends on only the phase difference between the two oscillators, $\phi(t) = \theta_2(t) - \theta_1(t)$.

The behavior of the pair of coupled oscillators depends critically and solely on the periodic interaction function chosen to represent the coupling. We can use our biophysical model to compute an interaction function $H(\phi)$ that is representative of a particular connection between two model cells. This is done by averaging the synaptic influence of the presynaptic cell over the cycle of a postsynaptic cell's oscillation. For a synaptic connection of the form provided in equation 3.2, the interaction function is

$$H(\phi) = \frac{1}{T}\int_0^T Z(t)(-\bar{g}_{Syn}S[V(t+\phi)](V(t) - V_{Syn}))dt. \tag{3.7}$$

The function $Z(t)$ is called the infinitesimal phase response curve (PRC). Thus, the net effect of this calculation is a convolution of the PRC with the function that describes the form of the synaptic coupling (Ermentrout, 1996).

The PRC is determined by the phase shifts that result from infinitesimally small perturbations during repetitive firing (Kuramoto, 1984; Hansel, Mato, & Meunier, 1995). It is possible to obtain a numerical computation that approximates this function (Ermentrout, 1996). A positive PRC indicates that a depolarizing perturbation at that time in the cycle will advance the phase of the oscillator, causing it to fire earlier. In contrast, a negative PRC indicates that a depolarizing perturbation will delay the phase, so the cell fires later. The function that describes the form of the synaptic coupling is chosen so that the resulting model synaptic current matches the experimental excitatory postsynaptic potentials recorded from a pyramidal cell in a slice preparation from layer Ib of rat olfactory cortex (Haberly & Bower, 1984). In this case, $\bar{g}_{Syn} = 1$ mS/cm^2, $V_{Syn} = 30$ mV, and the synaptic time course is equivalent to the dual exponential,

$$\alpha(t) = 2.75\frac{\exp(-t/\tau_1) - \exp(-t/\tau_2)}{\tau_1 - \tau_2}, \tag{3.8}$$

where $\tau_1 = 2.8$ and $\tau_2 = .65$. The resulting interaction function is insensitive to small changes in the form of the synaptic coupling; however, large changes in the synaptic time course can lead to a qualitative change in the dynamics of the coupled system (Crook, Ermentrout, & Bower, in press).

3.2 Phase-Locked Solutions. Once an interaction function has been computed, we use it to determine the phase-locked solutions to the simpler

coupled oscillator system. These are the solutions for which the phase difference $\phi(t) = \theta_2(t) - \theta_1(t)$ is constant. For example, $\phi(t) \equiv 0$ corresponds to the synchronous phase-locked solution. Determining the phase shift and stability of these solutions provides insight into the behavior of the more complicated biophysical system. From equations 3.5 and 3.7, we have

$$\frac{d\phi(t)}{dt} = \bar{g}(H(-\phi) - H(\phi)) \tag{3.9}$$

$$= -2\bar{g}H_{odd}(\phi), \tag{3.10}$$

since the even components cancel in the case of symmetric coupling. Any solution to the equation $d\phi(t)/dt = 0$ is a phase-locked solution to the system, so the phase-locked solutions correspond to the zeros of the odd component of the interaction function. Linearizing near a fixed solution $\bar{\phi}$, we obtain

$$\frac{d\phi(t)}{dt} \approx [-2\bar{g}H'_{odd}(\bar{\phi})]\phi(t). \tag{3.11}$$

When $[-2\bar{g}H'_{odd}(\bar{\phi})] < 0$, the solution is stable, so any particular phase-locked solution $\bar{\phi}$ is stable when $H'_{odd}(\bar{\phi}(t)) > 0$. Thus, we need only look at the form of the odd component of the interaction function near the zeros to predict the behavior of the system of two coupled cells (Ermentrout, 1996; Hansel, Mato, & Meunier, 1993).

4 Results

We compute the interaction functions that are representative of the behavior of two coupled model pyramidal cells for different levels of adaptation. The strength of the adaptation is varied by changing the maximal conductances of the currents responsible for adaptation in the biophysical model. First we eliminate the adaptation currents completely, compute the interaction function, and determine the phase-locked solutions. In this case, we find that the synchronous phase-locked solution is unstable. When we gradually strengthen the level of adaptation, we see a transition to stable synchrony. Figure 2 demonstrates this transition where the panels depict $H_{odd}(\phi)$ for two pyramidal cells coupled with excitatory synapses as the level of adaptation grows. Simulations of two synaptically coupled biophysical cell models verify that the behavior predicted by the coupled oscillator model holds for the biophysical model as well. Although the synchronous solution is unstable in the spiking model with excitatory coupling and no spike frequency adaptation, adding spike frequency adaptation to the cell model leads to stable synchrony. The simulation results are summarized in the schematic in Figure 3. Coupled oscillator models are valid when the coupling between oscillators is weak. The coupling parameter must also be smaller than all other parameters in the model. We use these biophysical simulations to verify that the same qualitative results hold for strong coupling as well and

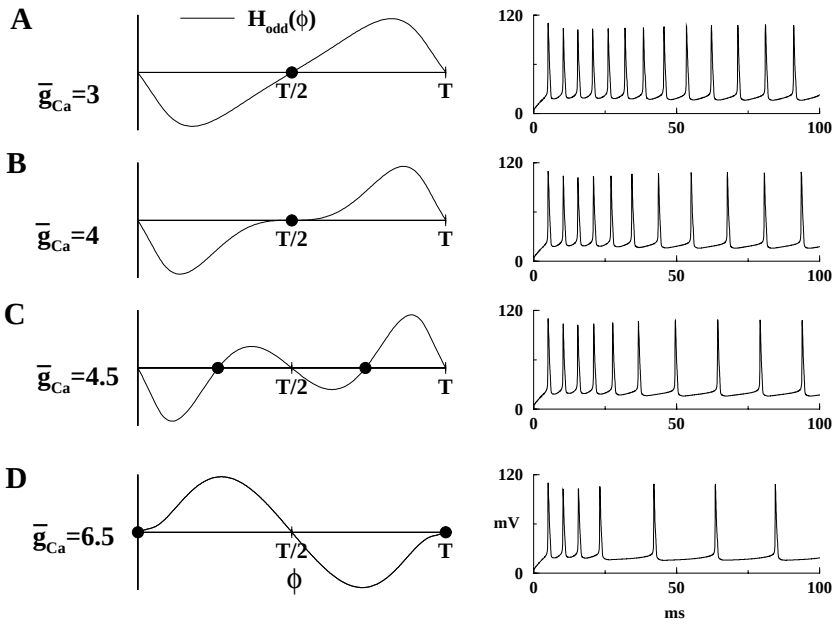

Figure 2: Odd part of the interaction function for two pyramidal cells coupled with excitatory synapses as the level of slow adaptation grows. The voltage traces on the right demonstrate the corresponding level of adaptation. Here we have set $\bar{g}_{K-M} = 0$, fixed $\bar{g}_{K-AHP} = 7$ mS/cm^2, and gradually increased the adaptive influence of I_{K-AHP} by increasing $\bar{g}_{Ca}$. We obtain the same transition if we eliminate I_{K-AHP} and vary $\bar{g}_{K-M}$. The phase difference ϕ lies between 0 and T where T ms is the period of the oscillation. Filled circles indicate stable phase-locked solutions. (A, B) In these panels, corresponding to lower levels of adaptation, the synchronous solution is unstable, and the antiphase solution is stable. (C) When the level of adaptation is large enough, there is a bifurcation so that two stable solutions appear near the antiphase solution. (D) High levels of adaptation lead to stable synchrony.

that the results are not affected by the size of the other parameters in the model.

Network simulations demonstrate that if the synchronous state of a pair of neurons is unstable, then a globally coupled network of such neurons cannot synchronize fully (Hansel et al., 1995). This is true for our pyramidal cell model when we perform simulations with a small network of model cells with symmetric all-to-all coupling. Figure 4 depicts the results for simulations with and without spike frequency adaptation. Panel A shows the

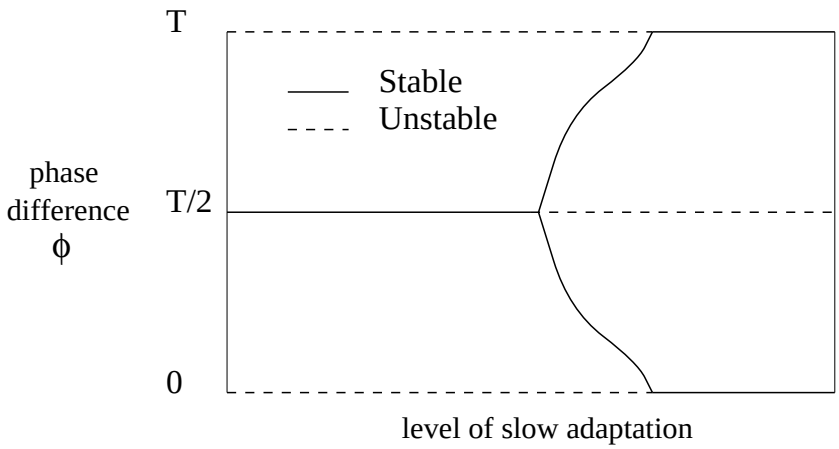

Figure 3: Schematic depicting the phase-locked solutions $\phi(t)$ for varying levels of slow adaptation. Solid curves and lines correspond to the stable phase-locked solutions, and dashed lines correspond to the unstable phase-locked solutions.

lack of synchrony inherent to networks of cells with no spike frequency adaptation, and panel B demonstrates the synchronizing properties of cells which include the slow processes for adaptation.

Ermentrout (1996) examines the solutions and the PRCs produced by depolarizing perturbations to type I spiking membrane models. He finds that these oscillators have nonnegative PRCs due to the fact that the minimum of the curve occurs at the spike. In this case, a depolarizing perturbation will always advance the phase of the oscillator, causing it to fire earlier. The analysis is valid whenever all dynamic processes are faster than the timescale of the period of the oscillation. This is the case in our model with no adaptation, as shown Figure 5E. Hansel et al. (1995) show that unless excitatory synapses are very fast, synchrony is not possible for excitatory coupling when the PRC is nonnegative. This is consistent with the lack of synchrony observed in our simulations of two model cells with no adaptation and only fast processes.

However, we find that in the presence of adaptation, the slow processes associated with the adaptation currents alter the dynamics so that the slope of the PRC is initially negative for our type I model. This leads to negative values on the portion the domain immediately following the action potential, as shown in Figure 5A. On this negative portion of the domain, a depolarizing perturbation will delay the phase of the oscillator, causing it to fire later. The delay occurs due to the high level of intracellular calcium

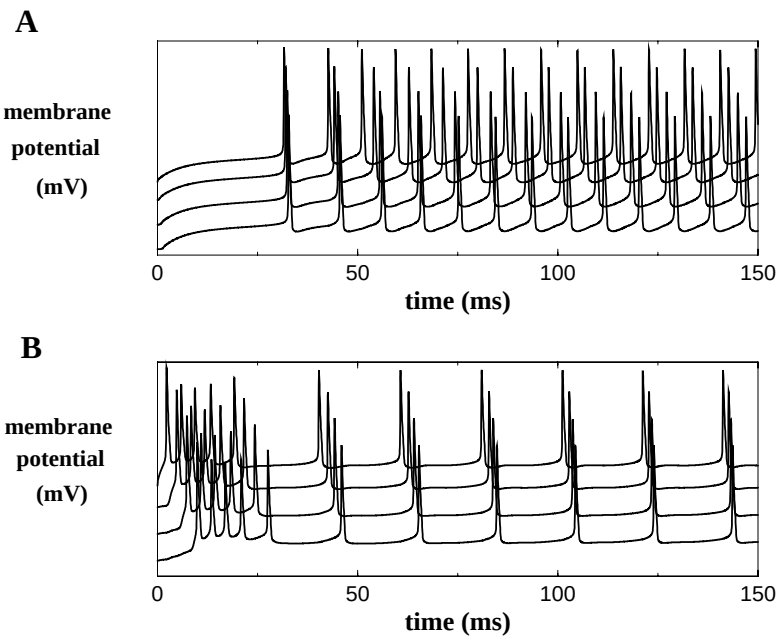

Figure 4: Voltage traces depicting the behavior of a small group of model pyramidal cells with symmetric all-to-all coupling. (A) The results for cells without spike frequency adaptation where synchronous initial conditions lead to out-of-phase behavior. (B) The results for model cells with weak spike frequency adaptation. The applied currents are begun at different times so that the cells are out of phase following adaptation; over time, the cells synchronize.

following each action potential, which allows a depolarizing perturbation to activate the hyperpolarizing adaptation currents. This difference in the PRC accounts for the change in behavior observed as we increase the level of adaptation. In the simulations of two coupled model cells with spike frequency adaptation, the phase of one model cell is advanced and the other is delayed until they are firing synchronously.

As expected, when we increase the speed of the processes that are responsible for adaptation, we find that the PRC becomes more similar to the one computed in the case of no adaptation. This is demonstrated in Figures 5B–D, where we scale the speed of the processes responsible for adaptation by 15, 30, and 45, respectively. The speed of the change in the voltage-gated I_{K-M} current is increased by scaling the equation for the change in the gating variable. In contrast, the intrinsic gating of the I_{K-AHP} current is rapid.

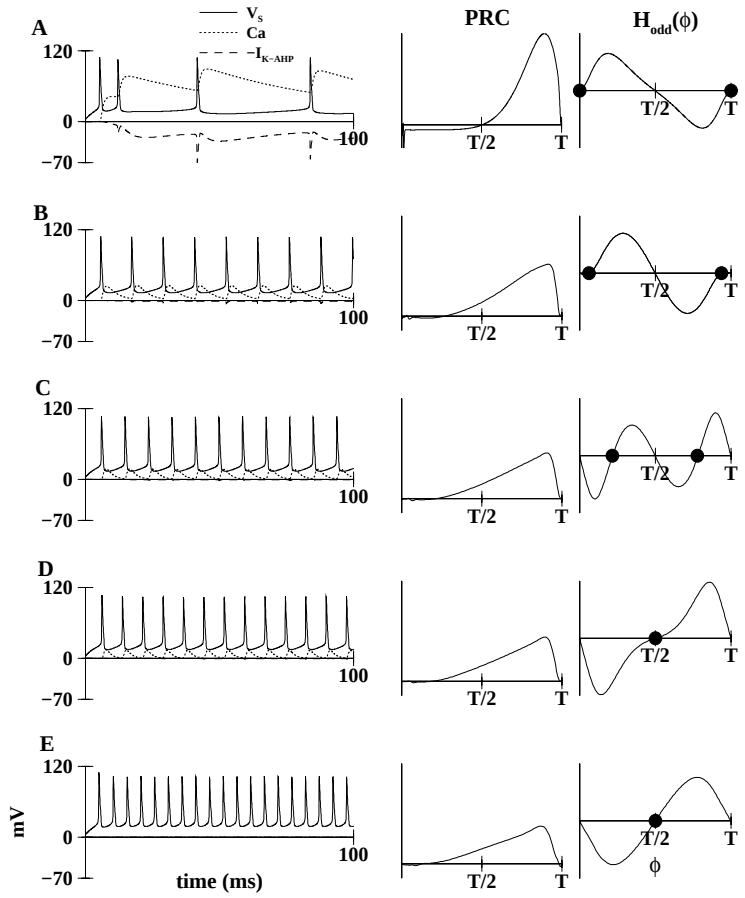

Figure 5: Membrane potentials, levels of intracellular calcium, and I_{K-AHP} currents in the model under varying circumstances with corresponding phase response functions and interaction functions shown on the right. Phase differences have been normalized to the period of oscillation for easy comparison, where the peak of the voltage oscillation occurs at time zero. Once again, filled circles indicate stable phase-locked solutions. (A) Results for the adapting model developed to match experimental data. (B–D) The equation for the gating variable for I_{K-M} and the term controlling the calcium depletion are scaled by 15, 30, and 45 respectively. (E) Results for the model with no adaptation. In the case of fast processes, the PRC is very similar to the one computed for the model with no adaptation. This demonstrates that the slow timescale of the adaptation is required for the change in behavior.

It is the kinetics of the intracellular calcium that determine the degree of adaptation (Lancaster & Zucker, 1994). Thus, this process is altered by increasing the speed of the depletion of intracellular calcium. The resulting changes in the interaction functions show that it is the slower processes that allow spike frequency adaptation to encourage the synchronization of cortical networks.

5 Discussion

Experimental evidence suggests that cholinergic drugs induce synchronous theta rhythm and gamma rhythm oscillations in electroencepalogram (EEG) recordings from hippocampus (Konopacki, MacIver, Bland, & Roth, 1987; Bland, Colom, Konopacki, & Roth, 1988) and olfactory cortex (Biedenbach, 1966). In these experiments, the typical cholinergic effect is an increase in the number of fast gamma oscillations seen in spontaneous EEG activity. In addition, the frequency of the slow theta rhythm decreases as the number of gamma oscillations increases. Traub, Miles, and Buzsáki (1992) replicate these effects in network biophysical simulations of hippocampus, and Barkai, Bergman, Horwitz, and Hasselmo (1994) do the same with simulations of olfactory cortex. In these models, cholinergic modulation is simulated with a reduction in the maximal conductances for the potassium currents responsible for adaptation. Decreasing the level of adaptation leads to an increase in the firing frequency of pyramidal cells. These slower outward adaptation currents are also responsible for setting the frequency of the slow rhythm, so cholinergic modulation, which reduces these currents, also causes a decrease in the frequency of the theta rhythm. The partial (not total) reduction in the level of adaptation is consistent with results that show partial recovery of this conductance during sustained application of acetylcholine (Benardo & Prince, 1982). Our result suggests that the remaining spike frequency adaptation is not only crucial for maintaining the slow rhythm in these simulations but is also necessary for the synchronization of the oscillations during periods of repetitive firing.

In the hippocampal model of Traub et al. (1992), the fast and slow inhibitory postsynaptic potentials are blocked. Thus, the network synchronization must be a product of the cellular properties and the excitatory coupling among pyramidal cells. Other models with intact spike frequency adaptation suggest that in some situations, synchronization may occur due to the influence of inhibitory interneurons (Traub, Miles, & Wong, 1987a; Traub, Miles, Wong, Schulman, & Schneiderman, 1987b; Traub et al., 1996). However, even in these models, which include inhibition, the network behavior is modified by the participation of pyramidal cells, and the spike frequency adaptation could contribute to the stability of the synchronous gamma oscillations.

More recent experimental results demonstrate a different mechanism in visual cortex and other neocortical areas (Munk, Roelfsema, König, Engel,

& Singer, 1996; Steriade, Amzica, & Contreras, 1996). In these areas, robust slow theta rhythms are present during drowsiness, deep sleep, and anesthesia; however, not much gamma activity is seen. With arousal, there is an increase in the release of acetylcholine, low-frequency theta oscillations diminish, and synchronous fast gamma-range oscillations are enhanced. Note that spike frequency adaptation can encourage synchrony even where it is too weak to cause the silent periods characteristic of the slower theta rhythm. This is evident in the simulation results shown in Figure 4B. Thus it is possible that spike frequency adaptation contributes to the stable synchronous oscillatory behavior in these areas as well.

It is worth noting that even in the presence of spike frequency adaptation, one should not assume that all excitatory connections among pyramidal cells are synchronizing. Delays such as the conduction delays introduced by lengthy axons (Crook et al., 1997) or even the delays introduced by distal excitatory synapses (Crook et al., in press) can introduce phase lags that prevent synchrony.

Appendix

Current Balance Equations

$$\begin{aligned} C_M\dot{V}_S &= -I_{Na}(V_S, m, h) - I_{K-DR}(V_S, n) - I_{Ca}(V_S, s, r) - I_{K-AHP}(V_S, q) \\ &\quad -I_{K-M}(V_S, w) - I_{L-S}(V_S) - g_c(V_S - V_D)/P + I_{Stim}/P \\ C_M\dot{V}_D &= -I_{L-D}(V_D) - g_c(V_D - V_S)/(1 - P), \end{aligned}$$

where V_S and V_D are the deviations of the somatic and dendritic membrane potentials from the reference potential of -77 mV, g_c is the coupling conductance parameter, and the current scaling parameter P is the proportion of the cell area taken up by the soma.

Ionic Currents

$$\begin{aligned} I_{Na}(V_S, m, h) &= \bar{g}_{Na} m^2 h (V_S - V_{Na}) \\ I_{K-DR}(V_S, n) &= \bar{g}_{K-DR} n (V_S - V_K) \\ I_{Ca}(V_S, s, r) &= \bar{g}_{Ca} s^2 r (V_S - V_{Ca}) \\ I_{K-AHP}(V_S, q) &= \bar{g}_{K-AHP} q (V_S - V_K) \\ I_{K-M}(V_S, w) &= \bar{g}_{K-M} w (V_S - V_K) \\ I_{L-S}(V_S) &= \bar{g}_{L-S} (V_S - V_L) \\ I_{L-D}(V_D) &= \bar{g}_{L-D} (V_D - V_L). \end{aligned}$$

Kinetic Equations The kinetic equations for the gating variables have the form $\dot{y}(u) = (y_\infty(u) - y(u))/\tau_y(u)$. The functions that determine the kinetic equations are listed below. In some cases we give the functions in

the form $\alpha_y(u)$ and $\beta_y(u)$ where $y_\infty(u) = \alpha_y(u)/(\alpha_y(u) + \beta_y(u))$ and $\tau_y(u) = 1/(\alpha_y(u) + \beta_y(u))$.

$$\alpha_m(V) = \frac{.32(30.1 - V)}{\exp(.25(30.1 - V)) - 1}$$
$$\beta_m(V) = \frac{.28(V - 57.1)}{\exp((V - 57.1)/5.0) - 1}$$
$$\alpha_h(V) = .128\exp((34 - V)/18)$$
$$\beta_h(V) = \frac{4}{\exp((57 - V)/5) + 1}$$
$$\alpha_n(V) = \frac{.059(52.1 - V)}{\exp((52.1 - V)/5) - 1}$$
$$\beta_n(V) = .925\exp(.925 - .025V)$$
$$\alpha_s(V) = \frac{.912}{\exp(-.072(V - 82)) + 1}$$
$$\beta_s(V) = \frac{.0114(V - 68.1)}{\exp((V - 68.1)/5) - 1}$$
$$\alpha_r(V) = \min(.005, .005\exp(-(V - 17)/20))$$
$$\beta_r(V) = (.005 - \alpha_r(V))$$
$$q_\infty(Ca) = (.0005Ca)^2$$
$$\tau_q(Ca) = \frac{.0338}{\min(.00001Ca, .01) + .001}$$
$$w_\infty(V) = \frac{1}{\exp(-(V - 42)/10) + 1}$$
$$\tau_w(V) = \frac{92\exp(-(V - 42)/20)}{1 + .3\exp(-(V - 42)/10)}$$

Calcium Handling

$$\frac{dCa}{dt} = -BI_{Ca} - Ca/\tau_{Ca}$$

where the variable Ca represents the intracellular free calcium level, $B = 3$, and $\tau_{Ca} = 60\ ms$.

Model Parameters. The maximal conductances in units of mS/cm^2 are $\bar{g}_{Na} = 221$, $\bar{g}_{K-DR} = 47$, $\bar{g}_{Ca} = 8.5$, $\bar{g}_{K-AHP} = 7$, and $\bar{g}_{K-M} = 6.5$. The maximal conductance of the leak current is $\bar{g}_{L-S} = 2$ in the soma compartment and $\bar{g}_{L-D} = .05$ in the dendrite compartment. The reversal potentials in units of mV are $V_{Na} = 132$, $V_K = -13$, $V_L = 0$, and $V_{Ca} = 197$. The capacitance is $C_M = .8\ \mu$F/cm^2. The coupling parameter is $g_c = 1.1$ mS/cm^2, and the current scaling parameter is $P = .05$.

Acknowledgments

This work was supported by the NIH and NIMH. We thank J. Rinzel, A. Sherman, and P. Latham for helpful discussion and comments. The reduced pyramidal cell model is available via ftp://www.nervana.montana.edu/pub/users/crook/pyr.ode.

References

Barkai, E., Bergman, R. E., Horwitz, G., & Hasselmo, M. E. (1994). Modulation of associative memory function in a biophysical simulation of rat piriform cortex. *Journal of Neurophysiology, 72*, 659–677.

Barkai, E., & Hasselmo, M. E. (1994). Modulation of the input/output function of rat piriform cortex pyramidal cells. *Journal of Neurophysiology, 72*, 644–658.

Benardo, L. S., & Prince, D. A. (1982). Ionic mechanisms of cholinergic excitation in mammalian hippocampal pyramidal cells. *Brain Research, 249*, 333–344.

Biedenbach, M. A. (1966). Effects of anesthetics and cholinergic drugs on prepyriform electrical activity in cats. *Experimental Neurology, 16*, 464–479.

Bland, B. H., Colom, L. V., Konopacki, J., & Roth, S. H. (1988). Intracellular records of carbachol-induced theta rhythm in hippocampal slices. *Brain Research, 447*, 364–368.

Bower, J. M. (1995). Reverse engineering the nervous system: An *in vivo*, *in vitro*, and *in computo* approach to understanding the mammalian olfactory system. In S. Zornetzer, J. Davis, and C. Lau (Eds.), *An introduction to neural and electronic networks* (pp. 3–28). San Diego: Academic Press.

Bressler, S. L. (1984). Spatial organization of EEGs from olfactory bulb and cortex. *Electroencephalography and Clinical Neurophysiology, 57*, 270–276.

Cohen, A., Ermentrout, G. B., Kiemel, T., Kopell, N., Sigvardt, K. A., & Williams, T. L. (1992). Modeling of intersegmental coordination in the lamprey central pattern generator for locomotion. *Trends in Neuroscience, 15*, 434–438.

Connors, B. W., Gutnick, M. J., & Prince, D. A. (1982). Electrophysiological properties of neocortical neurons *in vitro*. *Journal of Neurophysiology, 48*, 1302–1320.

Crook, S. M. (1996). *The role of delay in oscillatory models of olfactory cortex*. Unpublished doctoral dissertation, University of Maryland.

Crook, S. M., & Ermentrout, G. B. (1997). An analysis of the adaptive behavior of piriform cortex pyramidal cells. In *Computational neuroscience trends in research 1996*. New York: Plenum.

Crook, S. M., Ermentrout, G. B., & Bower, J. M. (In press). Dendritic and synaptic effects in systems of coupled cortical oscillators. *Journal of Computational Neuroscience*.

Crook, S. M., Ermentrout, G. B., Vanier, M. C., & Bower, J. M. (1997). The role of axonal delay in the synchronization of networks of coupled cortical oscillators. *Journal of Computational Neuroscience, 4*, 161–172.

Eeckman, F. H., & Freeman, W. J. (1990). Correlations between unit firing and EEG in the rat olfactory system. *Brain Research, 528*, 238–244.

Engel, A. K., König, P., Kreiter, A. D., Schillen, T. B., & Singer, W. (1992). Temporal coding in the visual cortex: New vistas on integration in the nervous system. *Trends in Neuroscience, 15*, 218–226.

Ermentrout, G. B. (1996). Type I membranes, phase resetting curves, and synchrony. *Neural Computation, 8*, 979–1001.

Ermentrout, G. B., & Kopell, N. (1984). Frequency plateaus in a chain of weakly coupled oscillators. *SIAM Journal on Mathematical Analysis, 15*, 215–237.

Ermentrout, G. B., & Kopell, N. (1990). Oscillator death in systems of coupled neural oscillators. *SIAM Journal of Applied Mathematics, 50*, 125–146.

Ermentrout, G. B., & Kopell, N. (1991). Multiple pulse interactions and averaging in systems of coupled neural oscillators. *Journal of Mathematical Biology, 29*, 195–217.

Freeman, W. J. (1978). Spatial properties of an EEG event in the olfactory bulb and cortex. *Electroencephalography and Clinical Neurophysiology, 44*, 586–605.

Gray, C. M. (1994). Synchronous oscillations in neuronal systems: Mechanisms and functions. *Journal of Computational Neuroscience, 1*, 11–38.

Gray, C. M., König, P., Engel, A. K., & Singer, W. (1989). Oscillatory responses in cat visual cortex exhibit inter-columnar synchronization which reflects global stimulus properties. *Nature, 338*, 334–337.

Gray, C. M., & Singer, W. (1987). Stimulus-specific neuronal oscillations in the cat visual cortex: A cortical functional unit. *Society of Neuroscience Abstracts, 13*, 404.3.

Gray, C. M., & Singer, W. (1989). Stimulus-specific neuronal oscillations in orientation columns of cat visual cortex. *Proceedings of the National Academy of Science, 86*, 1698–1702.

Haberly, L. B. (1985). Neuronal circuitry in olfactory cortex: Anatomy and functional implications. *Chemical Senses, 10*, 219–238.

Haberly, L. B., & Bower, J. M. (1984). Analysis of association fiber system in piriform cortex with intracellular recording and staining techniques. *Journal of Neurophysiology, 51*, 90–112.

Hansel, D., Mato, G., & Meunier, C. (1993). Clustering and slow switching in globally coupled phase oscillators. *Physical Review E, 48*, 3470–3477.

Hansel, D., Mato, G., & Meunier, C. (1995). Synchrony in excitatory neural networks. *Neural Computation, 7*, 192–210.

Hodgkin, A. L., & Huxley, A. F. (1952). A quantitative description of membrane current and its application to conduction and excitation in nerve. *Journal of Physiology (London), 117*, 500–544.

Konopacki, J., MacIver, M. B., Bland, B. H., & Roth, S. H. (1987). Carbachol-induced EEG "theta" activity in hippocampal brain slices. *Brain Research, 405*, 196–199.

Kuramoto, Y. (1984). *Chemical oscillations, waves, and turbulence*. New York: Springer-Verlag.

Lancaster, B., & Zucker, R. S. (1994). Photolytic manipulation of Ca^{2+} and the time course of slow, Ca^{2+}-activated K^+ current in rat hippocampal neurones. *Journal of Physiology London, 475*, 229–239.

Lanthorn, T., Storm, J., & Andersen, P. (1984). Current-to-frequency transduction in CA1 hippocampal pyramidal cells: Slow prepotentials dominate the primary range firing. *Experimental Brain Research, 53*, 431–443.

Madison, D. V., & Nicoll, R. A. (1984). Control of the repetitive discharge of rat CA1 pyramidal neurones *in vitro*. *Journal of Physiology, London, 354*, 319–331.

McCormick, D. A., Connors, B., Lighthall, J., & Prince, D. A. (1985). Comparative electrophysiology of pyramidal and sparsely spiny stellate neurons of the neocortex. *Journal of Neurophysiology, 54*, 782–806.

Munk, M. H. J., Roelfsema, P. R., König, P., Engel, A. K., & Singer, W. (1996). Role of reticular activation in the modulation of intracortical synchronization. *Science, 272*, 271–274.

Pinsky, P. F., & Rinzel, J. (1994). Intrinsic and network rhythmogenesis in a reduced Traub model for CA3 neurons. *Journal of Computational Neuroscience, 1*, 39–60.

Rinzel, J., & Ermentrout, G. B. (1992). Analysis of neural excitability. In C. Koch & I. Segev (Eds.), *Methods in neuronal modeling* (pp. 135–169). Cambridge, MA: MIT Press.

Segev, I., Fleshman, J. W., & Burke, R. E. (1992). Compartmental models of complex neurons. In C. Koch & I. Segev (Eds.), *Methods in neuronal modeling* (pp. 63–96). Cambridge, MA: MIT Press.

Sherman, S. M., & Koch, C. (1986). The control of retinogeniculate transmission in the mammalian lateral geniculate nucleus. *Experimental Brain Research, 63*, 1–20.

Steriade, M., Amzica, F., & Contreras, D. (1996). Synchronization of fast (30–40 Hz) spontaneous cortical rhythms during brain activation. *Journal of Neuroscience, 16*, 392–417.

Steriade, M., & Llinas, R. R. (1988). The functional states of the thalamus and the associated neuronal interplay. *Physiology Review, 68*, 649–742.

Traub, R., Miles, R., & Buzsáki, G. (1992). Computer simulation of carbachol-driven rhythmic population oscillations in the CA3 region of the *in vitro* rat hippocampus. *Journal of Physiology, 451*, 653–672.

Traub, R., Miles, R., & Wong, R. (1987a). Models of synchronized hippocampal bursts in the presence of inhibition. I. Single population events. *Journal of Neurophysiology, 58*, 739–751.

Traub, R., Miles, R., Wong, R., Schulman, L. S., & Schneiderman, J. H. (1987b). Models of synchronized hippocampal bursts in the presence of inhibition. II. Ongoing spontaneous population events. *Journal of Neurophysiology, 58*, 752–764.

Traub, R. D., Wittington, M. A., Stanford, I. M., & Jefferys, J. G. R. (1996). A mechanism for generation of long-range synchronous fast oscillations in the cortex. *Nature, 383*, 621–624.

Traub, R., Wong, R., Miles, R., & Michelson, H. (1991). A model of a CA3 hippocampal pyramidal neuron incorporating voltage-clamp data on intrinsic conductances. *Journal of Neurophysiology, 66*, 635–649.

Vanier, M. C., & Bower, J. M. (1996). A comparison of automated parameter-searching methods for neural models. In J. M. Bower (Ed.), *Computational neuroscience* (pp. 477–482). San Diego: Academic Press.

Whittington, M. A., Traub, R. D., & Jefferys, J. G. R. (1995). Synchronized oscillations in interneuron networks driven by metabotropic glutamate receptor activation. *Nature, 373*, 612–615.

Wilson, M., & Bower, J. M. (1991). A computer simulation of oscillatory behavior in primary visual cortex. *Neural Computation, 3*, 498–509.

Wilson, M., & Bower, J. M. (1992). Cortical oscillations and temporal interactions in a computer simulation of piriform cortex. *Journal of Neurophysiology, 67*, 981–995.

Received June 9, 1997; accepted October 2, 1997.